

國立交通大學
資訊科學與工程研究所

碩士論文



研究生：粘家盛

指導教授：易志偉 教授

中華民國 101 年 6 月

用於路面異常偵測之智慧型手機探偵車系統
Smartphone-based Probe Car System for Road Abnormality Detection

研究 生：粘家盛

Student : Chia-Sheng Nian

指導 教授：易志偉

Advisor : Chih-Wei Yi

國立交通大學
資訊科學與工程研究所
碩士論文

A Thesis
Submitted to Institute of Computer Science and Engineering
College of Computer Science
National Chiao Tung University

in partial Fulfillment of the Requirements
for the Degree of
Master
in

Computer Science

June 2012

Hsinchu, Taiwan, Republic of China

中華民國 101 年 6 月

國立交通大學

博碩士論文全文電子檔著作權授權書

(提供授權人裝訂於紙本論文書名頁之次頁用)

本授權書所授權之學位論文，為本人於國立交通大學資訊科學與工程研究所 _____組，100 學年度第 2 學期取得碩士學位之論文。

論文題目：用於路面異常偵測之智慧型手機探偵車系統

指導教授：易志偉

■ 同意

本人茲將本著作，以非專屬、無償授權國立交通大學與台灣聯合大學系統圖書館：基於推動讀者間「資源共享、互惠合作」之理念，與回饋社會與學術研究之目的，國立交通大學及台灣聯合大學系統圖書館得不限地域、時間與次數，以紙本、光碟或數位化等各種方法收錄、重製與利用；於著作權法合理使用範圍內，讀者得進行線上檢索、閱覽、下載或列印。

論文全文上載網路公開之範圍及時間：

本校及台灣聯合大學系統區域 網路	<input checked="" type="checkbox"/> 中華民國 106 年 8 月 11 日 公開
校外網際網路	<input checked="" type="checkbox"/> 中華民國 106 年 8 月 11 日 公開

■ 全文電子檔送交國家圖書館

研究生：粘家盛 (親筆簽名)

指導教授：易志偉 (親筆簽名)

中華民國 101 年 8 月 13 日

國立交通大學

博碩士紙本論文著作權授權書

(提供授權人裝訂於全文電子檔授權書之次頁用)

本授權書所授權之學位論文，為本人於國立交通大學資訊科學與工程研究所 _____組，100 學年度第 2 學期取得碩士學位之論文。

論文題目：用於路面異常偵測之智慧型手機探偵車系統

指導教授：易志偉

同意立即公開

本人依著作權法第15條第2項第3款之規定(採推定原則即預設圖書館得公開上架閱覽)，同意將本著作，以非專屬、無償授權國立交通大學，基於推動讀者間「資源共享、互惠合作」之理念，與回饋社會與學術研究之目的，國立交通大學圖書館得以紙本收錄、重製與利用；於著作權法合理使用範圍內，讀者得進行閱覽或列印。

不同意立即公開

1. 本論文為本人向經濟部智慧局申請專利的附件之一，申請文號為：申請中，請將論文延至____年____月____日再公開。

2. 本論文已投稿期刊並待審核中，請將論文延至____年____月____日再公開。

說明：配合教育部函(100年7月1日臺高(二)字第1000108377號)，紙本不公開期限以5年為限

研究生：粘家盛 (親筆簽名)

本人已了解以上內容

指導教授：易志偉 (親筆簽名)
中華民國 101 年 8 月 13 日

國家圖書館

博碩士論文電子檔案上網授權書

(提供授權人裝訂於紙本論文本校授權書之後)

ID:GT079955608

本授權書所授權之論文為授權人在國立交通大學資訊科學與工程研究所 100 學年度第 2 學期取得碩士學位之論文。

論文題目：用於路面異常偵測之智慧型手機探偵車系統

指導教授：易志偉

茲同意將授權人擁有著作權之上列論文全文（含摘要），非專屬、無償授權國家圖書館，不限地域、時間與次數，以微縮、光碟或其他各種數位化方式將上列論文重製，並得將數位化之上列論文及論文電子檔以上載網路方式，提供讀者基於個人非營利性質之線上檢索、閱覽、下載或列印。

※ 讀者基於非營利性質之線上檢索、閱覽、下載或列印上列論文，應依著作權法相關規定辦理。

論文全文上載網路公開之範圍及時間：2017.8.11 公開。

研究生：粘家盛 (親筆簽名)

指導教授：易志偉 (親筆簽名)

中華民國 101 年 8 月 13 日

國立交通大學
研究所碩士班

論文口試委員會審定書

本校 資訊科學與工程 研究所 粘家盛 君

所提論文：

用於路面異常偵測之智慧型手機探偵車系統

Smartphone-based Probe Car System for Road Abnormality
Detection

合於碩士資格水準、業經本委員會評審認可。

口試委員：翁村杰 孫敏徑

易志偉

指導教授：易志偉

所長：

徐勝中

中華民國 101 年 7 月 20 日

用於路面異常偵測之智慧型手機探偵車系統

學生：粘家盛

指導教授：易志偉 教授

國立交通大學

資訊科學與工程研究所

摘要

道路品質的優劣與民眾乘載交通工具的舒適、安全與速度有著重要的影響，對於騎乘自行車與機車的民眾而言，更是影響甚多。然而對於道路品質優劣依據卻沒有一個考量到科學性、便利性、以及經濟性的方法。因此本論文提出以智慧型手機探偵車系統用於偵測路面異常點，並針對路面異常點進行分級，以期望能以較客觀的方式鑑定道路品質的優劣。一般車輛行經異常顛簸路段，例如：人孔蓋、低窪坑洞、減速丘、伸縮縫時，車輛本身會受到垂直方向的震動，因此車輛本身所受到的震動影響可作為判斷車輛是否行經顛簸路段。此外，我們考慮到影響震動幅度的因素，例如裝置置放於不同車架、不同車輛的懸吊系統、不同感測器的誤差和不同的車速等，因此單純震動的幅度並不足夠做為路面品質的客觀指標。我們提出一個異常偵測演算法，利用車輛行駛於路面異常點時震動標準差除以行駛一般正常道路時震動標準差的參考值，作為異常點大小分級。結果顯示，我們的演算法能夠消除影響震動幅度的因素，並針對異常點大小分級。

關鍵字：智慧型手機探偵車、行動感測、路面品質偵測。

Smartphone-based Probe Car System for Road Abnormality Detection

Student : Chia-Sheng Nian

Advisors : Dr. Chih-Wei Yi

Institute of Computer Science and Engineering
National Chiao Tung University

Abstract

Road quality is an important index for modern traffic networks. It affects not only traffic flows but also safety and comfortableness of passengers. However, there are no scientific, convenient and economical methods to evaluate the road quality. In this work, we propose a smartphone-based probe car system that utilizes mobile sensing to pervasively detect road abnormality such as potholes, speed bumps, expansion joints, manhole covers, etc. Since the vibration caused by an abnormality mainly affects in the vertical direction of a vehicle, in our system, the road abnormalities are detected by vibration measured in embedded inertial measurement units (IMUs) of onboard smartphones. However, there are many factors such as orientation of smartphones, phone racks, sensor chips of smartphones, types of vehicles, driving speed, etc., which affect the vibration sensed by the smartphones. Therefore, several mechanisms are proposed to overcome these challenges including a vertical component extraction algorithm and an abnormality detection algorithm by the vibration characteristic (the standard deviation of vertical vibration) and the grade of the abnormality is obtained. The result indicates that our algorithm can eliminate these factors and grade the road abnormality.

Keywords : Smartphone-based probe car, mobile sensing, road abnormality detection.

誌 謝

我要感謝我的指導教授，易志偉教授，在我碩士生涯這兩年給我很多的指導跟鼓勵，並且提供了我良好的實驗室環境，讓我得以順利完成此篇論文。

再來，我由衷的感謝我的指導學長莊宜達，在研究上提供很多建議與指導。另外，也感謝網路最佳化實驗室(NOL)的全體同學，在這兩年來給我的鼓勵與幫助。

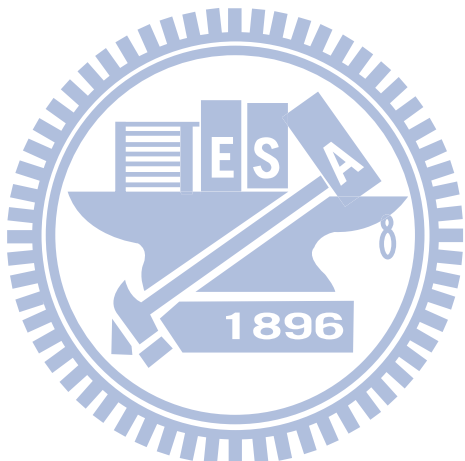
最後，我要感謝我的父母以及所有關心我的人對我付出的關懷與期許，使我在挫折的時候可以再度站起來，度過最困難的時光。真的謝謝大家，因為有你們的幫忙跟鼓勵，讓我在碩士兩年的生涯學到很多也經歷很多，留下許多美好的回憶。謝謝！



Contents

1	Introduction	1
1.1	Backgrounds and Motivations	1
1.2	Research Goals	3
1.3	Organization	4
2	Related Works	6
2.1	Road Abnormality Detected by High Sampling Rate Devices	6
2.2	Road Abnormality Detected by Low Sampling Rate Devices	8
3	Road Abnormality Detection	10
3.1	Waveform Caused by Abnormalities	12
3.2	Vertical Component Extraction Module	14
3.3	Abnormality Detection Algorithm	18
3.4	Clustering Algorithm	21
4	Field Trial Experiments and Results	23

4.1	Devices and Data Formats	24
4.2	Relation between the Speed and the Standard Deviation of Vertical Acceleration	27
4.3	Abnormality Detection	30
4.3.1	Abnormal Waveform Verification	31
4.3.2	NCTU Campus Scenario	33
4.3.3	Xin'an Road Scenario	34
4.4	Modification of the Detection Algorithm by Underdamped Oscillation Model	37
5	Conclusions	43



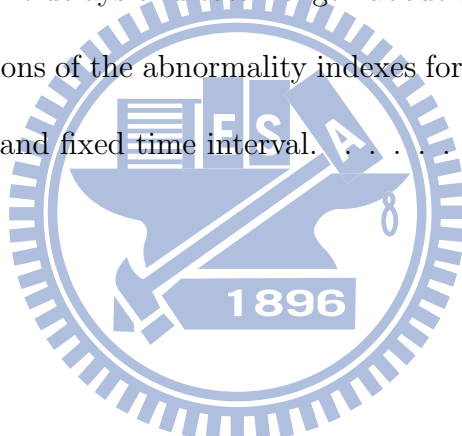
List of Figures

3.1	The road abnormality detection framework.	11
3.2	The waveform is vibration as vehicle passing an abnormality.	12
3.3	The duration of the main wave.	14
3.4	The flow chart of the vertical component extraction process.	17
3.5	The waveforms of the z-axis sensor readings and the vertical components obtained by the batch mode and the online mode.	19
3.6	The RMSE to the vertical components by the batch mode for different smart-phones with different T	19
4.1	(a) Rack R_1 , (b) Rack R_2 , (c) Rack R_3	26
4.2	The standard deviation at different speeds.	27
4.3	Test site in the NCTU campus scenario.	28
4.4	The relation between the duration of the main wave and the vehicle speed in the NCTU campus scenario.	29
4.5	The relation between the standard deviation of the main wave and the vehicle speed in the NCTU campus scenario.	29

4.6	Test site in the Xin'an Road Scenario.	30
4.7	The relation between the standard deviation of the main wave and the vehicle speed in the Xin'an Road Scenario.	31
4.8	(a):vehicle vibration at a speed of 8m/s, (b):vehicle vibration at a speed of 5.5m/s	32
4.9	Results of bump detection in the NCTU campus scenario.	34
4.10	The AI for different speeds with respect to different racks. (a) AI derived by $\frac{\sigma_{event}^{\perp}}{\sigma^{\perp}}$. (b) AI derived by $\frac{\sigma_{event}^{\perp}}{\sigma_j^{\perp}}$	35
4.11	Results of expansion joints detection in the Xin'an Road Scenario.	36
4.12	The relation between the multiples and the vehicle speed on the scenario 2.	36
4.13	The abnormality index between different type abnormalities.	37
4.14	The abnormality index measured by HTC Desire under (a) unfixed time interval Δt and (b) fixed time interval Δt	39
4.15	The abnormality index for expansion joints measured by HTC Desire under (a) unfixed time interval Δt and (b) fixed time interval Δt	40
4.16	The abnormality index for expansion joints measured by Sony Xperia S under (a) unfixed time interval Δt and (b) fixed time interval Δt	41
4.17	The average abnormality index for (a) bumps and (b) expansion joints.	42

List of Tables

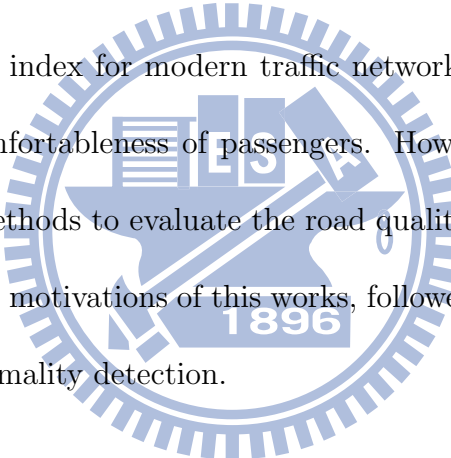
4.1	Accelerometer Differences between android smartphones	26
4.2	Standard Deviation between different states in the NCTU campus scenario. .	28
4.3	Error between different delays and total length about $3.6m$	33
4.4	The standard deviations of the abnormality indexes for bumps and expansion joints under unfixed and fixed time interval.	39



Chapter 1

Introduction

Road quality is an important index for modern traffic networks. It affects not only traffic flows but also safety and comfortableness of passengers. However, there are no scientific, convenient and economical methods to evaluate the road quality. In this Chapter, we introduce current backgrounds and motivations of this works, followed by our goals and proposed framework for the road abnormality detection.



1.1 Backgrounds and Motivations

Road networks that connect buildings, villages, cities, and even countries are the most important civic infrastructure for transportation. From the aspect of road users, the quality of roads is related to not only driving experience but also driving safety. Driving on a bad-condition road at a high speed incurs serious shaking and even skid of vehicles that may cause damage to mechanical parts, decrease the lifetime of vehicles, and sometimes induce

traffic accidents. To avoid the potential hazards or uncomfortableness, drivers will slow down their speeds and result in reducing the average traffic speed.

On the other hand, from the aspect of governments, the quality of roads is one of the most observable metrics to evaluate the performance of governments. To improve the image of governments, they are willing to spend a large amount of money to construct and maintain road infrastructure. Every year, a large portion of budget is allocated for such a purpose. For example, Taipei City Government has been launching a multiple year project [1] to improve the quality of roads and remove bumps and potholes. The main tasks include (1) intensifying the robustness of roadbed; (2) covering manholes to increase the flatness of roads; (3) routine road inspection and pothole repairment; and (4) unregulated maintenance to response requests from citizens. 2 billion NT dollars (around 66 million US dollars) in 2009 and 2.58 billion NT dollars (around 86 million US dollars) in 2010 were budgeted for this project. Although the project has been undergoing for several years, arguments about the efficiency and even effectiveness of the project still exist among citizens. Furthermore, commissioners must be sent by the government to inspect the road conditions in the city area every day, but it spends a lot of humanresources for achieving in real-time. A scientific evaluation system is therefore needed for monitoring the road quality in real-time and objectively evaluating the performance and improvement of projects.

The driving experience may be affected by many road conditions such as obstacles, bumps on roads, potholes, manholes, speed ramps, manhole covers, etc. In the following discussion, we call them road abnormalities in general. Recently, there are many works on road abnor-

mality detection [2][3][4][5]. To detect an abnormality on roads, inertial measurement units (IMUs) such as accelerometers are installed in a vehicle to measure the vibration while the vehicle moves over the road and an abnormality is detected based on the magnitude of the vibration.

1.2 Research Goals

Motivated by the story and related works given above, we consider how to measure the quality of roads by integration of smartphones and vehicles. Smartphones providing various sensing capabilities and communication interfaces give a good platform in vehicles, which forms probe cars for the abnormality detection. In this work, we try to use the concept of the smartphone probe car to pervasively collect road quality information in a long-term manner. Our major objectives include

- Provide a scientific evaluation system and metrics to fairly evaluate the quality of roads.
- Provide the capability to detect the existence of new road abnormalities in short time so that the authority can send officers to investigate the abnormality and apply necessary repair procedure as fast as possible.

The road abnormality in this work is detected by the vibration measured by the IMU embedded in the smartphone. However, there are many factors that affect the vibration sensed by the smartphones, readings from the IMU are needed to be well preprocessed to

obtain correct vibration information. For example, a vibration caused by an abnormality mainly affects in the vertical direction of the vehicle. So, if the smartphone is not placed in a proper position, the sensor readings may not reveal the actual vertical vibration. Phone racks, sensor chips of smartphones and types of vehicles may affect the vibration sensed by the smartphone. In addition, different driving speeds cause different severity of vibration on the same abnormality. To overcome these challenges, several mechanisms are proposed. A vertical component extraction algorithm is used to obtain the vertical vibration such that users do not need to be careful about the orientation of their smartphones. An abnormality detection algorithm is proposed by comparing the vibration characteristic in an abnormality with that in a stable state to eliminate diversity effects of phone racks, sensors chips of smartphones and types of vehicles. To eliminate the diversity effect on driving speeds, the vibration characteristics measured in different speeds are applied and the grade of each abnormality is obtained. Finally, the information of the abnormality such as location can be uploaded to a cloud server and the detected road quality information can be combined with position information by Global Positioning System (GPS)[6][7][8] and then upload to servers for further processing and applications.

1.3 Organization

The rest of this thesis is organized as follows. Chapter 2 covers some related works. The proposed framework for road abnormality detection is presented in Chapter 3. The field trial experiment results of our framework is provided in Chapter 4. Conclusions are drawn

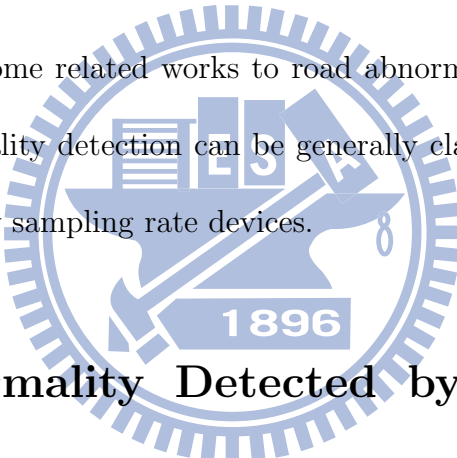
in Chapter 5.



Chapter 2

Related Works

In this Chapter, we review some related works to road abnormality detection. In general, the works related to abnormality detection can be generally classified to detection by high sampling rate devices and low sampling rate devices.



2.1 Road Abnormality Detected by High Sampling Rate Devices

The preliminary work on road abnormality detection was introduced in [2]. The authors proposes a road condition detection and environmental monitoring system on the public transport system called BusNet [2]. A Crossbow MICAz mote[9] is installed in a bus which combines several sensors such as a GPS receiver, a tri-axial accelerometer, a thermometer and a carbon monoxide sensor to detect the road surface condition and monitor environmental

pollution. Buses going around cities collect sensed data and data are gathered in bus stations while the buses entering the station. They focus on how the data are collected while the bus entering to the stations without discussing details about how bumps are detected and the vibration factors.

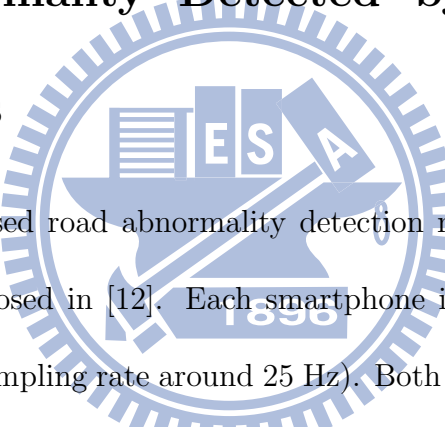
Followed by [3], a mobile sensor network-based system for road surface and monitoring called Pothole Patrol is proposed. An external accelerometer (sampling rate 380Hz) and an external GPS receiver are installed in a taxi and sensed data are gathered to a notebook over Bluetooth. The system adopts a client-server architecture in which vehicle clients process raw data to produce detected events and report these events to a central sever where clustering is performed to filter false alarms. To detect bumps, various filter algorithms are proposed based on speed, frequency of vibration, the peak of vertical vibration, the ratio of horizontal to vertical vibration and speed to vertical vibration ratio. In addition, events close in distance are clustered together or are treated as noises if there is not sufficient number of events in the same cluster. The placement of the device is considered for attaching to dashboard, windshield and embedded PC, but the orientation of the device is restricted to be aligned to the same orientation of the vehicle.

After that handheld devices are involved in the detection in [4] called Nericell. Various handheld devices, including the packet PC[10], the cellular phone and the accelerometer (sampling rate up to 600Hz)[11], are installed in a vehicle to detect traffic and road condition such as honking events for the severity of traffic chaos and bumps for the quality of roads. The packet PC is the computing center of the system, the cellular phone with a GPS receiver and

a microphone is the source for location information and audio data, and the accelerometer is used to detect bumps. A threshold-based bump detection algorithm is proposed, the z-sus vibration is used when the vehicle moves at a high speed ($\geq 25\text{kmph}$) and the z-peak vibration is used when the vehicle moves at a slow speed ($< 25\text{kmph}$). A virtually reorienting algorithm based on Eular angles is proposed to deal with the orientation between devices and the vehicle. However, the reorientation algorithm needs the help of extra devices and the vibration factor issues are not addressed.

2.2 Road Abnormality Detected by Low Sampling

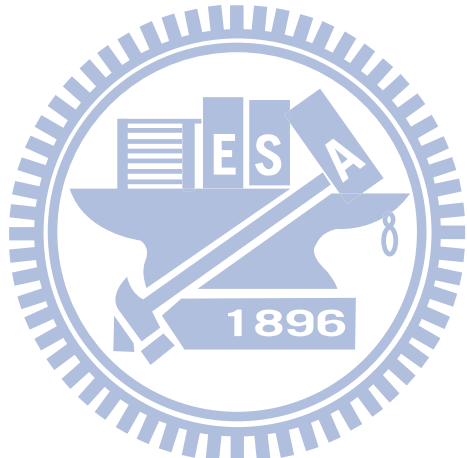
Rate Devices



Later, a machine learning-based road abnormality detection method which adopts smartphones in motorcycles is proposed in [12]. Each smartphone is embedded with a GPS receiver and a accelerometer (sampling rate around 25 Hz). Both supervised and unsupervised learning methods are proposed for road anomaly detection. For supervised learning method, a re-labeling mechanism for training data is proposed. For unsupervised learning method, a clustering-based method is proposed to obtained threshold for road abnormality detection. They assumes the device is placed with the same orientation of the vehicle. To evaluate road quality, a road quality index based on the roughness index for road quality assessment is defined. The problem of this method is that the orientation of devices is restricted and both supervised and unsupervised learning method need large amounts of data to create

abnormality detection model.

In [5], four threshold-based methods for road abnormality detection are proposed. The Z-THRESH method checks the vertical vibration, the Z-DIFF method detects by the difference of consecutive vertical vibration, the STDEV(Z) method determines by the standard deviation of the vertical vibration in a window, and the G-ZERO method detects whether the sensor senses $0G$ vibration. The threshold is determined by tuning it with the best detection results. However, if the system adopts different devices, it needs to retrain their system parameters.



Chapter 3

Road Abnormality Detection

In this chapter, we present our road abnormality detection framework. Figure 3.1 shows the framework which consists of three modules: vertical component extraction module, abnormality detection module and clustering module. The input of the framework is the vibration caused by road abnormality which is measured as acceleration by the G-sensor. The vertical component extraction module is required for extraction of acceleration magnitude of vertical vibration from sensor readings. Then, the abnormality detection module takes the vertical acceleration for road abnormality detection and produces abnormality features. Finally, the clustering module groups abnormalities with the same type by their location information to eliminate possible noise. Before we discuss the details about the modules in the framework, we investigate the vibration waveform caused by the abnormality first.

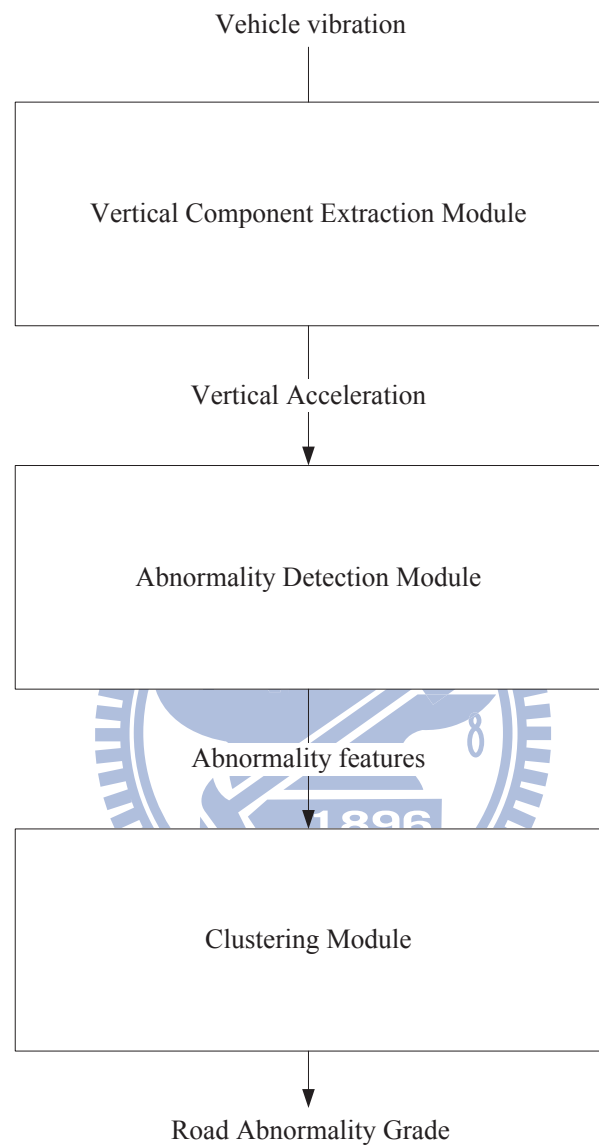


Figure 3.1: The road abnormality detection framework.

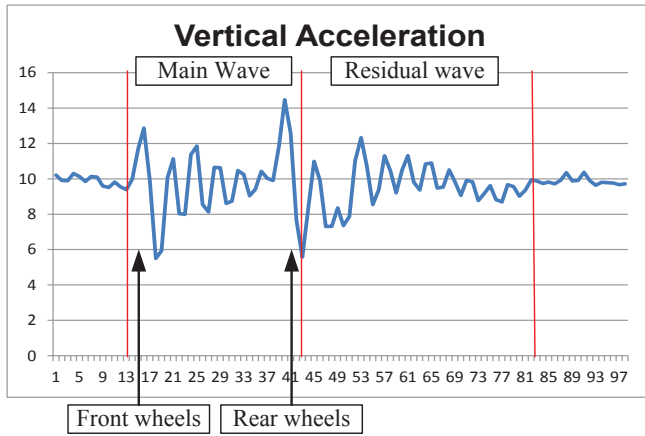


Figure 3.2: The waveform is vibration as vehicle passing an abnormality.

3.1 Waveform Caused by Abnormalities

In this section, a preliminary investigation about the vibration waveform of acceleration caused by the abnormality is conducted. Fig 3.2 is a typical vibration wave detected by a HTC desire[13] smartphone with a sampling rate $48Hz$ installed on a rack in a vehicle. The vehicle moves over a bump at a speed of $22.5km/hr$. In the figure, a 2-second waveform of the vibration is recorded in terms of the vertical acceleration measured in m/s^2 with respect to the sample number. The wave can be divided into two distinct waves: a main wave and a residual wave. The duration of the main wave is from the time when front wheels hit the bump to the time after rear wheels hit it. A wave beginning at sample number 13 to 17 is caused when the front wheels hit the bump and another wave beginning at sample number 37 to 41 is caused when the rear wheels hit the bump. The duration of the residual wave is the time after the rear wheels hit the bump (at sample number 43) to the time when the

vehicle enters to stable state at sample number 82). The residual wave reflects the fact that the rack keeps oscillating after both front and rear wheels hit the bump. The durations of the main wave and the residual wave are affected by *vibration factors* such as phone racks, suspension system of vehicles, sensor chips of smartphones, driving speed, etc.

Fig 3.3 illustrates a vehicle moves over a pothole and the corresponding waveform during the impact process. Let the duration of the main wave denoted by Δt . The front wheels hit the pothole at time t_f followed by the rear wheels hit at time t_r . So, the duration of the main wave $\Delta t = t_r - t_f$. However, it is not easy to determine t_f and t_r , especially when the vehicle moves at a high speed. To find Δt , we observe that the displacement of a vehicle during the impact process equal to the sum of the wheelbases l_w and the dimension of the abnormality l_a . Δt can therefore be expressed by

$$\Delta t = \frac{l_a + l_w}{v} \quad (3.1)$$

Since the dimension of the abnormality is unknown, the nominator of Eq. (3.1) can be approximated by the average length of the wheelbase which is $4m$.

The vibration detected by smartphone during stable state and when the vehicle hits an abnormality can be analog to an under-damped oscillation[14][15][16]. The acceleration sensed by smartphones reflects the grade of the vibration and can be expressed by

$$a(t) = A e^{-\lambda t} \cos(\omega t) \quad (3.2)$$

where A is the maximum amplitude, $\omega = \sqrt{\frac{k}{m} - \frac{b^2}{4m^2}}$ is the angular frequency and $\lambda = \frac{b}{2m}$ is distortion rate. m , k and b are the mass of the smartphone, the spring coefficient and the

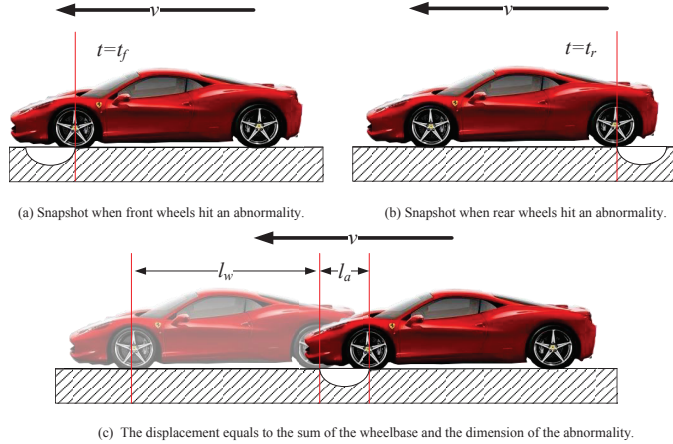


Figure 3.3: The duration of the main wave.

damping coefficient, respectively. In order to alleviate the vibration factors, the standard deviation[17] (3.3) of the acceleration instead of the magnitude of the acceleration to detect abnormalities. Then, we calculate the ratio that is the standard deviation of the scalar of sensor readings during when the vehicle hits an abnormality divided by the standard deviation during stable state to represent the magnitude of abnormalities.

$$\sigma = A \sqrt{\left(\frac{1}{\Delta t} \int_0^{\Delta t} (e^{-\lambda t} \cos(\omega t))^2 dt - \left(\frac{1}{\Delta t} \int_0^{\Delta t} e^{-\lambda t} \cos(\omega t) dt \right)^2 \right)} \quad (3.3)$$

3.2 Vertical Component Extraction Module

The vibration caused by abnormality mainly reflects on acceleration along the vertical direction. However, since a smartphone and a vehicle is temporally coupled, the vertical component of acceleration can not be directly obtained from sensor readings. A process is

needed to extract the acceleration magnitude in the vertical direction from the sensor readings. Let \mathbf{g} , \mathbf{a} and \mathbf{G} , respectively, be the sensor reading of a G-sensor, the acceleration of the object and the gravity, the relation between them can be expressed by

$$\mathbf{g} = \mathbf{a} - \mathbf{G} + \epsilon \quad (3.4)$$

where ϵ is error of the G-sensor.

According to Eq. (3.4), if the sensor is in a stable state, *i.e.*, $\mathbf{a} = \mathbf{0}$, we have $\mathbf{g} = -\mathbf{G} + \epsilon$. In addition, if ϵ is negligible, then $-\mathbf{g}$ is a good estimator of \mathbf{G} can be estimated by $-\mathbf{g}$. To decide whether a sensor is in a stable state, it is possible to verify whether $\|\mathbf{g}\| - \|\mathbf{G}\|$ less than a threshold. However, due to inaccuracy of sensors, $\|\mathbf{G}\|$ is different from sensors to sensors. So, it is not easy to determine the threshold. We propose to use standard deviation of the scalar of \mathbf{g} in the vertical direction to find the stable state. Let U denote the set of the sensor readings collected in one second and Σ^\perp be the standard deviation of the scalar of \mathbf{g} in the vertical direction. This second is called a *stable period* if $\forall \mathbf{g} \in U$ such that $\|\text{proj}_{\mathbf{g}_0} \mathbf{g}\| - \|\mathbf{g}_0\| < \Sigma^\perp$, where $\text{proj}_{\mathbf{g}_0}$ is a projection function[18] to project a vector \mathbf{g} on \mathbf{g}_0 . Assume ϵ is a zero mean noise, to alleviate the effect of ϵ , we take the average on \mathbf{g} over stable periods. Figure 3.4 shows the flow chart of the proposed process. Let U_{T_0} , U_i , U_i^\perp , U^\perp , S and S^\perp , respectively, be the set of sensor readings in the first T_0 seconds, the set of sensor readings in the $(T_0 + i)$ -th second, the set of sensor readings in the vertical direction in the $(T_0 + i)$ -th second, the set of sensor readings in the vertical direction for last T_1 seconds, the set of sensor readings during stable periods for last T_1 seconds and the set of sensor readings in the vertical direction during stable periods for last T_1 seconds.

At the beginning, sensor readings in the first T_0 seconds are collected in U_{T_0} , $S = U_{T_0}$, $U^\perp = S^\perp = \{\mathbf{proj}_{\mathbf{g}_0} \mathbf{g} | \mathbf{g} \in U_{T_0}\}$, $\mathbf{g}_0 = \mathbf{avgv}$ and $\Sigma^\perp = \mathbf{stdev}_{\mathbf{v} \in U^\perp} \|\mathbf{v}\|$. Later on, for every second, the sensor readings is collected in U_i , $U_i^\perp = \{\mathbf{proj}_{\mathbf{g}_0} \mathbf{g} | \mathbf{g} \in U_i\}$, $U^\perp = U^\perp \cup U_i^\perp$ and Σ^\perp is updated with the new U^\perp . If the sensor readings are collected for more than T_1 seconds, then the oldest one-second sensor readings are removed from S , S^\perp and U^\perp . If this second is a stable period, then $S = S \cup U_i$, $S^\perp = S^\perp \cup U_i^\perp$ and $\sigma^\perp = \mathbf{stdev}_{\mathbf{v} \in S^\perp} \|\mathbf{v}\|$ where σ^\perp is the standard deviation of the scalar of sensor readings during stable periods for last T_1 seconds. We will discuss the usage of σ^\perp later. Last, \mathbf{g}_0 is updated with the new S if this second is a stable period.

To evaluate the vertical component extraction process, an experiment was performed by a vehicle driving on a highway from 13:07:36 ~ 13:36:28 on June 15th 2012. A Sony Xperia S smartphone with sampling rate $80Hz$ placed inside the vehicle and orthogonal to the ground is used in the experiment. A batch mode and an online mode of the process are evaluated in the experiment. In the batch mode, \mathbf{g}_0 is obtained by taking average on \mathbf{g} over all stable periods whereas, in online mode, \mathbf{g}_0 is obtained by where $T_1 = 60$ seconds. In the experiment, z-axis sensor readings are compared to that projected on \mathbf{g}_0 estimated by the batch mode and the online mode. Figure 3.5 shows waveforms of z-axis sensor readings, vertical accelerations by projecting the sensor readings on \mathbf{g}_0 estimated in the batch mode and the online mode of the process where horizontal axis is time domain measured in millisecond and vertical axis is acceleration measured in m/s^2 . The waveform in the top is for the z-axis sensor readings, the one in the middle and the bottom are for the batch mode and online mode, respectively.

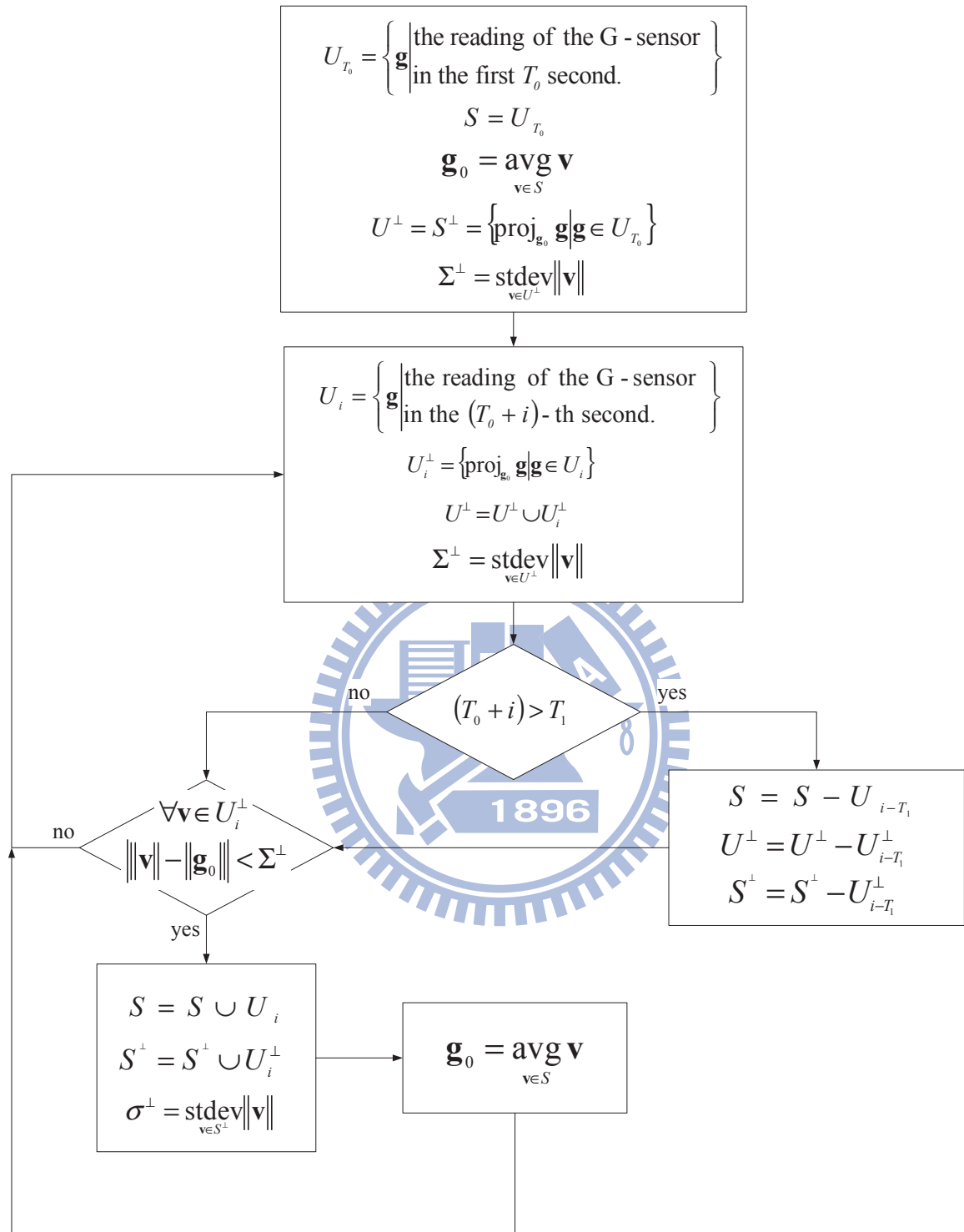


Figure 3.4: The flow chart of the vertical component extraction process.

It can be seen that both waveforms extracted by the process have almost the same shape to the z-axis values. In addition, the RMSEs to the z-axis values are 0.01 m/s^2 for the batch mode and 0.03 m/s^2 for the online mode.

Since the orientation of a smartphone may be changed time by time (For example, a phone may drop from a rack.), we further investigate the effect of T_1 . An similar experiment with different T_1 (from 10 seconds to 90 seconds) was performed by taking three smartphones with different orientations. Two HTC desire (sampling rate $48Hz$) and one HTC hero (sampling rate $46Hz$) smartphones are used in this experiment. In addition, one HTC desire is on a rack and the other two are sticked on a windshield. Vertical components obtained by projecting the sensor readings on \mathbf{g}_0 from the batch mode is taken as the basement in this experiment since the RMSE to the z-axis values for the batch mode in the previous experiment is within the error bound of the device (0.01 m/s^2). Figure 3.6 illustrates the RMSE to the vertical components by the batch mode for different smartphones with different T_1 . The result shows that with a larger T_1 yields a smaller RMSE from . So, we choose $T_1 = 60$ seconds based on this result for later analysis.

3.3 Abnormality Detection Algorithm

Recall the previous discussion about the related works, the devices adopted in the experiments are monotonic. In other words, they do not consider factors that affect the abnormality detection. For example, different vehicles have different suspension systems, different racks have different quality, different sensor chips have different accuracy, moving speeds, all af-

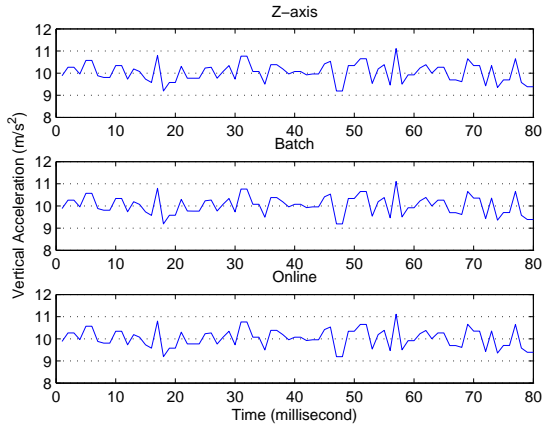


Figure 3.5: The waveforms of the z-axis sensor readings and the vertical components obtained by the batch mode and the online mode.

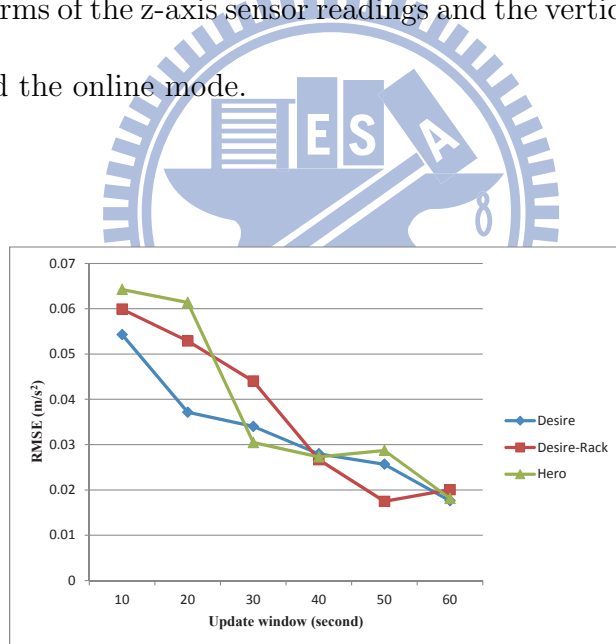


Figure 3.6: The RMSE to the vertical components by the batch mode for different smartphones with different T .

fект the abnormality detection. In addition, the thresholds used in their algorithms only reflect some specific experiment environment. Once the experiment environment changes (a different smartphone or different orientation or different moving speeds), they have to find another threshold to satisfy the changed environment. To increase the capability of abnormality detection algorithm on different environments, we use the ratio of the standard deviation of the main wave, σ_{event}^\perp , and the standard deviation of the sensor reading during stable periods, σ^\perp as the abnormality index. Further, to reduce the affection of moving speed, σ^\perp introduced in Section 3.2 is splitted into m groups $\{\sigma_1^\perp, \sigma_2^\perp, \sigma_j^\perp, \dots, \sigma_m^\perp | 1 \leq j \leq m\}$ by the speed.

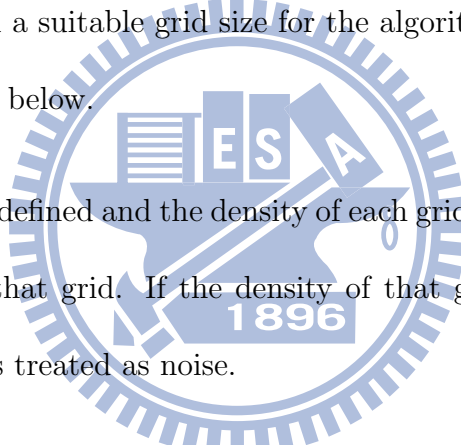
The algorithm is presented below:

1. For each sensor reading g_i , we check whether the difference of the scalar of vertical component of g_i ($\|\mathbf{proj}_{g_0} g_i\|$) and g_0 is greater than is greater than the standard deviation of the acceleration in the vertical direction, Σ^\perp .
2. If step 1 satisfies, an abnormality is detected. The duration of main wave Δt is calculated by 3.1. Let $U_{\Delta t}^\perp$ be the set of vertical accelerations measured during the duration of the main wave. The standard deviation of main wave is calculated by $\sigma_{event}^\perp = \text{stdev}_{\mathbf{v} \in U_{\Delta t}^\perp} \|\mathbf{v}\|$. The abnormality index for this event is calculated by $AI = \frac{\sigma_{event}^\perp}{\sigma_j^\perp}$ where σ_j^\perp is the standard deviation during stable period corresponding to the moving speed .
3. The information of detected abnormality event including AI , latitude, longitude and timestamp is uploaded to the server.

3.4 Clustering Algorithm

Due to location drifting problem of GPS, there may have spatial error occurring on the location information of a detected abnormality event. So, abnormalities of the same type may fall within a small circle rather than a point. To solve this problem, a clustering algorithm is proposed by grouping abnormalities of the same type that are spatially close to each other to the same abnormality. We use a grid-based clustering algorithm called DENCLUE [19][20] in this work. The grid-base clustering algorithm is more efficient than other clustering algorithm on computing. Since the spatial diversity of abnormalities is insignificant, it is easy to find a suitable grid size for the algorithm.

The algorithm is sketched below.



1. The suitable grid size is defined and the density of each grid is calculated by the number of abnormal events in that grid. If the density of that grid is less than a threshold $MinCluster$, the grid is treated as noise.
2. We find the grid with the maximum density as the density attractor. The density attractor forms a cluster. The adjacent grids of the density attractor are absorbed by the density attractor, if the density between the adjacent grid and the density attractor is less than a threshold D .
3. If there are still grids not be tested, go back to Step 2. Otherwise, the clustering procedure is done. The resulted clusters represent distinguished abnormalities and the location of the abnormality is determined by the average of the location of abnormality

in the cluster.



Chapter 4

Field Trial Experiments and Results

The proposed abnormality detection framework was verified via a series of field trial experiments. We first introduce devices using in the experiment including smartphones and racks and the data format used in the work. Then, to demonstrate the relation between the speed and the standard deviation of vertical acceleration, series of experiments were conducted in a highway scenario, the road surrounding NCTU campus and Xin'an road. Later, we verify the relation of duration of main wave of an abnormality (for example, bumps), the dimension of that abnormality and the moving speed in the road surrounding NCTU campus. After that the abnormality detection (for example, bumps and expansion joints) experiments were performed in the road surrounding the campus and Xin'an road, to show the accuracy of our framework, followed by the modification of the detection algorithm by underdamped oscillation.

4.1 Devices and Data Formats

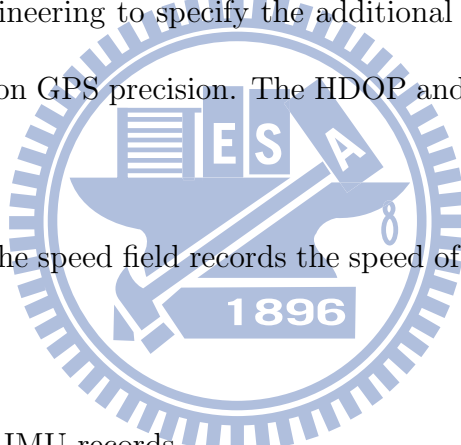
There are three different types of smartphones including HTC Desire, HTC Hero and Sony Xperia S. The GPS sampling rate is set to $1Hz$. The accelerometers of different smartphones have different sampling rate as shown in Table 4.1. Three different racks R_1 , R_2 and R_3 are used in the experiment as shown in Figure 4.1. There are two types of data sets including the GPS data and IMU data recorded in the experiment. For the GPS data, there are ten fields, including data type, time stamp, fix quality, latitude, longitude, altitude, HDOP, VDOP, and speed. The GPS data mainly adopt from what used in the National Marine Electronics Association standard NMEA-0169. For the IMU data, there are fourteen fields, including data type, time stamp, acceleration (including accX, accY, accZ), magnetic field (including magX, magY, magZ), angle speed (including angX, angY, angZ), and Euler angle (including roll, pitch and yaw). The details are introduced below.

- Fields used in both GPS and IMU records

- Data Type (0 or 1): The field identifies the data type of the entry, 0 for GPS data and 1 for IMU data.
 - Time (hhmmss or F.stamp): The time field stores the time of the entry. The time field used in the GPS data records follows Coordinated Universal Time (UTC), but the time field used in the IMU data records is the system time clock in floating number format.

- Fields used only by the GPS records

- Fix Quality (0 or 1): The fix quality field is used for the data validation, 0 for invalid, 1 for GPS fix and 2 for DGPS fix, the value is either 0 or 1 in the experiment tracking logs.
- Latitude, Longitude and Altitude (F.lat, F.lng, F.alt): These fields represent the position of a vehicle in the geographic coordinate system. All these fields are floating numbers.
- HDOP and VDOP (F.hdop, F.vdop): These fields respectively represent the horizontal and vertical dilution of precision (DOP), and DOP is a term used in GPS and geomatics engineering to specify the additional multiplicative effect of GPS satellite geometry on GPS precision. The HDOP and VDOP fields are in floating number format.
- Speed (F.speed): the speed field records the speed of a vehicle in floating number format.



- Fields used only by the IMU records

- AccX, AccY and AccZ (F.accX, F.accY, F.accZ): These fields are the acceleration measured by an accelerometer in m/sec^2 for three axes of the accelerometer. The acceleration fields are floating numbers.
- MagX, MagY and MagZ (Fs.magX, Fs.magY, Fs.magZ): These fields are ambient magnetic measured by a magnetic meter in μ -Tesla for three axes of the magnetic meter. The magnetic fields are floating numbers in scientific notation.

Table 4.1: Accelerometer Differences between android smartphones

Device	Sampling rate	Z-axis StdDev (m/s^2)
HTC Hero	$46Hz$	0.041087487
HTC Desire	$48Hz$	0.052942531
Sony Xperia S	$80Hz$	0.030425036

- AngX, AngY and AngZ (0.0, 0.0, 0.0): These fields are the rate of rotation around the device’s three axes in rad/sec . The rotation speed fields are all zero in the experiment log.
- Roll, Pitch and Yaw (0, 0, 0): These fields indicate the Euler angles for the device’s three axes. The Euler angle fields are all zero in the experiment log.



Figure 4.1: (a) Rack R_1 , (b) Rack R_2 , (c) Rack R_3

4.2 Relation between the Speed and the Standard Deviation of Vertical Acceleration

The purpose of this experiment is to check whether the standard deviations (Σ^\perp , σ^\perp and $\sigma_{\perp\perp}$) is larger as the vehicle speed is getting faster. We choose three test sites including a road segment of highway from Hsinchu to Jubei and a road surrounding NCTU campus and Xin'an Road for data collection.

In the high way scenario, two HTC desire and two HTC hero smartphones are used in this experiment on June 15, 2012. One HTC desire is installed on rack R_3 , and the rests are stucked to a windshield. The moving speeds are separated to 8 groups. Figure 4.2 shows the results of Σ^\perp to different speeds with respect to different smartphones. It can be seen that Σ^\perp is larger as the vehicle speed is getting faster. In the NCTU campus scenario (Figure

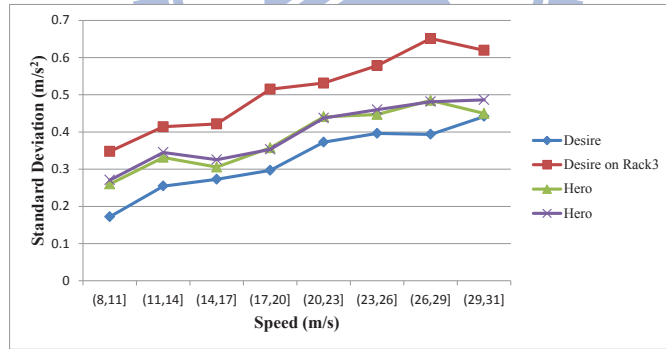


Figure 4.2: The standard deviation at different speeds.

4.3), two HTC desire smartphones on rack R_1 and R_2 are placed in the front and rear seat on May 22, 2012. We drive a vehicle at a speed between $10km/hr$ and $30km/hr$ along a

Table 4.2: Standard Deviation between different states in the NCTU campus scenario.

Standard Deviation	R_1	R_2
Σ^\perp	1.0288726181794	0.70020709606504
σ^\perp	0.31201088378631	0.18179924664677
$\sigma_{[4,7)}^\perp$	0.34957717653201	0.23103789025174
$\sigma_{[7,10)}^\perp$	0.37861965199194	0.24992372448386

road surrounding NCTU campus. We calculate Σ^\perp and σ^\perp for two different types of racks as shown in Table 4.2. It can be seen that for different types of racks have different values of Σ^\perp and σ^\perp . The relation between v and standard deviation of main wave σ_{event}^\perp is shown in Figure 4.5. It shows that σ_{event}^\perp is larger as the vehicle speed is faster and different types of smartphones have different vibration due to different racks.



Figure 4.3: Test site in the NCTU campus scenario.

In the Xin'an Road Scenario (As shown in Figure 4.6), two HTC desire, two HTC hero

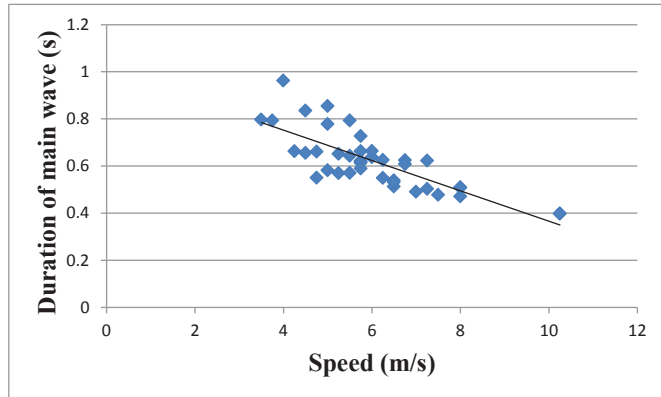


Figure 4.4: The relation between the duration of the main wave and the vehicle speed in the NCTU campus scenario.

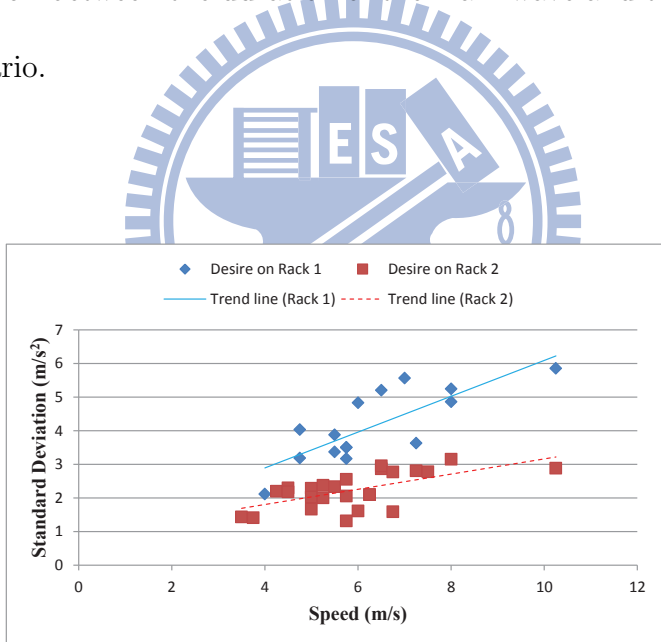


Figure 4.5: The relation between the standard deviation of the main wave and the vehicle speed in the NCTU campus scenario.

and two Sony Xperia S smartphones are installed in the experiment on June 5, 2012. One HTC desire, one HTC hero and one Sony Xperia S are installed on the rack R_1 , R_3 and R_2 respectively, and other smartphonnes are adhered to window glass by twin adhesive. As shown in Figure 4.6, we drive a vehicle from A to B to collect data at different speeds of $20km/hr$, $40km/hr$ and $60km/hr$. The vehicle takes U turns at B and continue another round of data collection. Totally, there are four rounds performed in the experiment. As same as analysis of scenario 1, we analyze relation between σ_{event}^\perp and v as show in Fig 4.7. The result is also the same as scenario 1, which means σ_{event}^\perp is larger as vehicle speed is faster.



Figure 4.6: Test site in the Xin'an Road Scenario.

4.3 Abnormality Detection

We next evaluate the proposed framework on the abnormality detection in the NCTU campus scenario and Xin'an Road scenario. The evaluation in this section includes abnormal

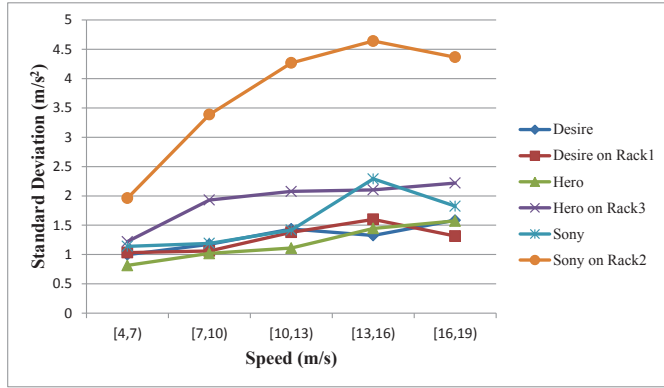
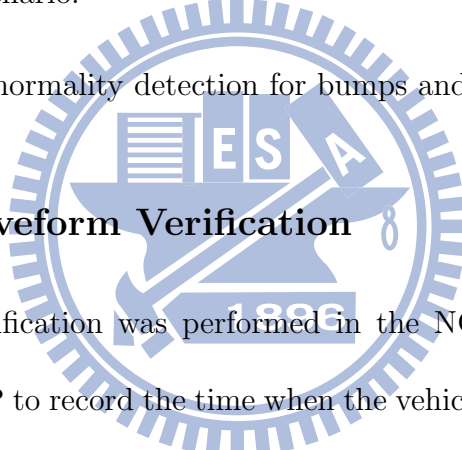


Figure 4.7: The relation between the standard deviation of the main wave and the vehicle speed in the Xin'an Road Scenario.

waveform verification and abnormality detection for bumps and expansion joints.



4.3.1 Abnormal Waveform Verification

The abnormal waveform verification was performed in the NCTU campus scenario. We develop a data collection APP to record the time when the vehicle hits a bump. The relation between the vehicle speed v and the duration of main wave Δt is shown in Figure 4.4. It can be seen that Δt is getting smaller as the speed increases. Figure 4.8 further illustrates the relation between Δt and v . It also shows that the vibration is getting serious as the vehicle speed increases.

The duration of main wave Δt by equation 3.1 is verified. Since the speed obtained by GPS has delay due to the nature of GPS, we take into account the GPS delay and calculate the total length of $l_a + l_w$ by the product of Δt and v measured at different delays (from 0

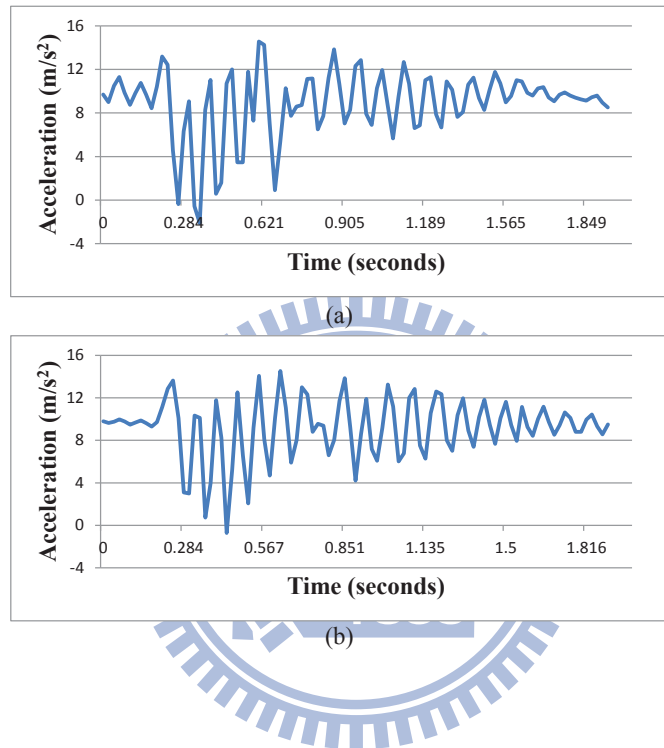


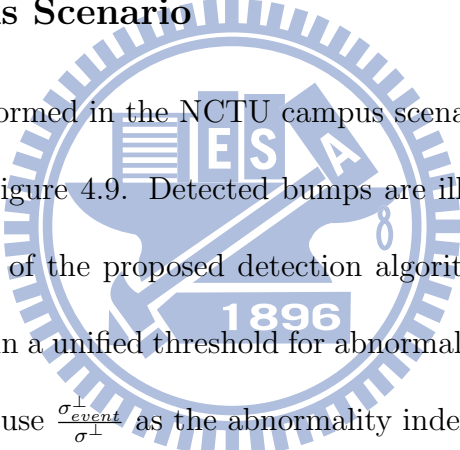
Figure 4.8: (a):vehicle vibration at a speed of 8m/s , (b):vehicle vibration at a speed of 5.5m/s

Table 4.3: Error between different delays and total length about 3.6m

	No delay	Delay 1 second	Delay 2 seconds
Average ($v * \Delta t$)	3.63405625	3.60731875	3.573352241
Error	0.95%	0.20%	0.74%

second to 2 seconds). We measure the width of bumps which is 0.5m and the wheelbase of the vehicle is 3.1m, and the error between different delays and total length about 3.6m as shown in Table 4.3.

4.3.2 NCTU Campus Scenario



The bump detection was performed in the NCTU campus scenario and the detection result after clustering is shown in Figure 4.9. Detected bumps are illustrated by balloons in the map. To show the capability of the proposed detection algorithm on reducing the factors that affect vibration and obtain a unified threshold for abnormality detection under different experiment environments, we use $\frac{\sigma_{event}^\perp}{\sigma_j^\perp}$ as the abnormality index and the result is shown in Figure 4.10 (a). It shows that the abnormality index has similar trend line on different type racks but the trend line for Desire on Rack 1 has greater slope than that on Desire on Rack 2. This is caused by the moving speed. To further reduce the speed factor, we split σ^\perp into two groups by speeds in the ranges [4, 7) and [7, 10) (σ_1^\perp for speeds in [4, 7) and σ_2^\perp for speeds in [7, 10)) and calculate the abnormality index by $\frac{\sigma_{event}^\perp}{\sigma_j^\perp}$. The result is shown in Figure 4.10 (b). It can be seen that the slope of trend line for the abnormality index is smoother than that in Figure 4.10 (a).



Figure 4.9: Results of bump detection in the NCTU campus scenario.

4.3.3 Xin'an Road Scenario

The expansion joints detection was performed in the Xin'an Road scenario. The detection results and the positions of expansion joints after clustering are shown in Figure 4.6. The width of expansion joint is $0.9m$ and the wheelbase of our car is $3.1m$, so we use the time interval Δt calculated by $l_a + l_b$ to calculate σ_{event}^\perp . Then, we use $\frac{\sigma_{event}^\perp}{\sigma^\perp}$ as the abnormal index and the result is shown in Fig 4.12(a). It shows a similar result as compared to Figure 4.10 (a). Similarly, to reduce the speed factor, we split σ^\perp into five groups by speeds in the ranges $[4, 7)$, $[7, 10)$, $[10, 13)$, $[13, 16)$ and $[16, 19)$ (σ_1^\perp for speeds in $[4, 7)$, σ_2^\perp for speeds in $[7, 10)$, ...) and calculate the abnormality index by $\frac{\sigma_{event}^\perp}{\sigma_j^\perp}$. The result is shown in Figure 4.12 (b).

At the end of this section, we demonstrate the unity of the abnormality index by averaging the abnormality index of bumps and expansion joints with respect to different speed. The

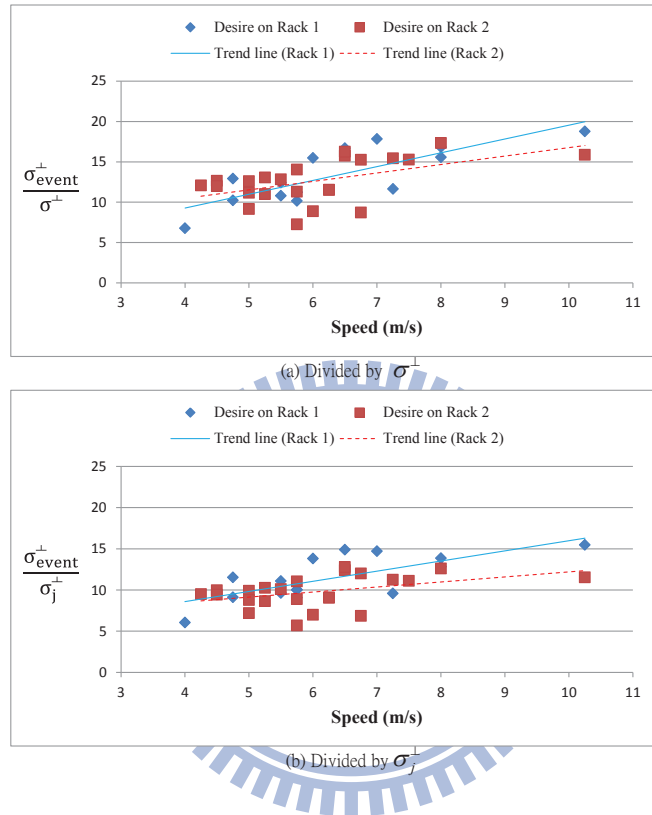


Figure 4.10: The AI for different speeds with respect to different racks. (a) AI derived by $\frac{\sigma_{\text{event}}^\perp}{\sigma^\perp}$. (b) AI derived by $\frac{\sigma_{\text{event}}^\perp}{\sigma_j^\perp}$.



Figure 4.11: Results of expansion joints detection in the Xin'an Road Scenario.

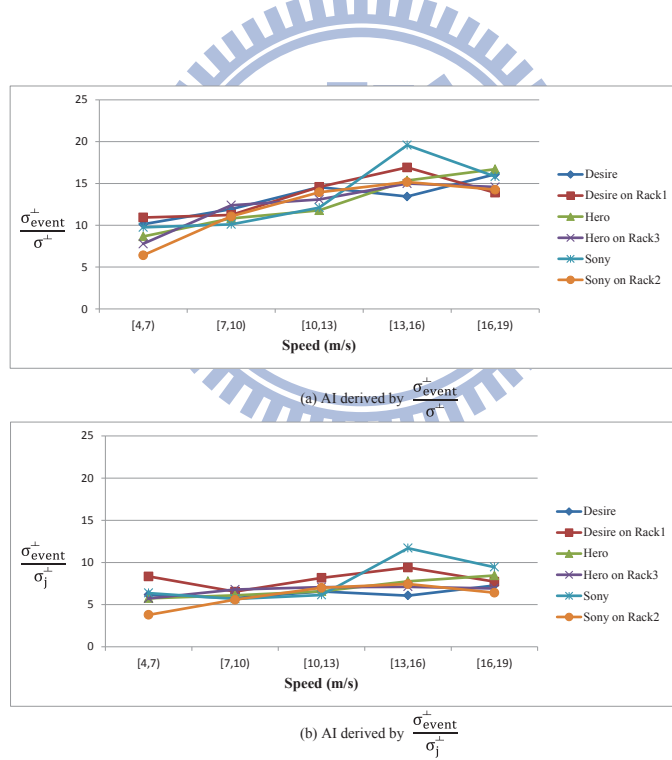


Figure 4.12: The relation between the multiples and the vehicle speed on the scenario 2.

result is shown in Fig 4.13. It can be seen that different types of abnormalities have different abnormality indexes. For example, the index for bump is 10.2283 and the index for expansion joint is 6.7886.

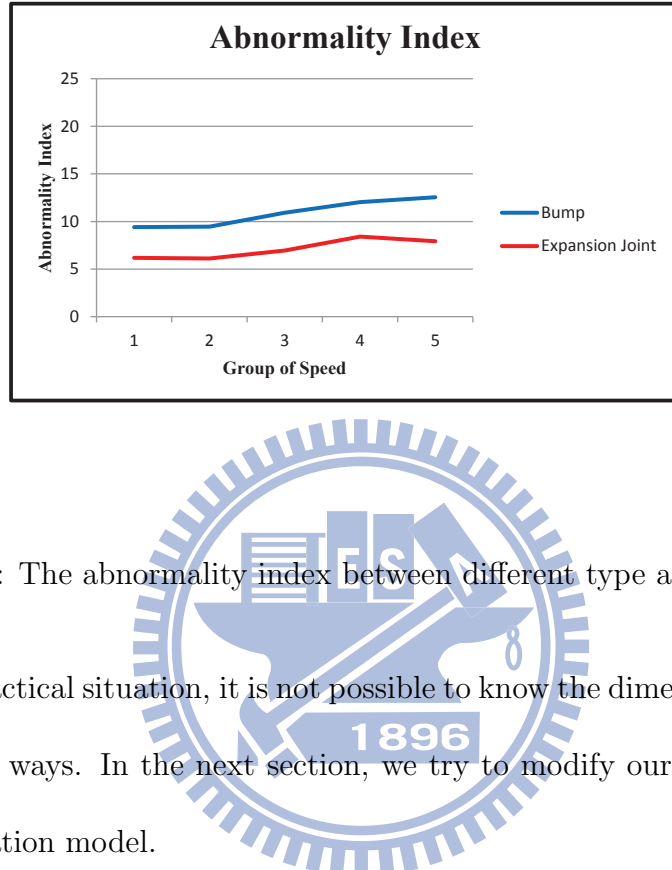


Figure 4.13: The abnormality index between different type abnormalities.

However, in a practical situation, it is not possible to know the dimension of abnormalities without any specific ways. In the next section, we try to modify our method by using the underdamped oscillation model.

4.4 Modification of the Detection Algorithm by Underdamped Oscillation Model

Recall in Section 3.1, we know that main waves and vibrations during stable period can be analog to underdamped oscillation. We calculate the abnormality index by $\frac{\sigma_{event}^\perp}{\sigma_j^\perp}$, which can

be expressed by

$$\frac{\sigma_{event}^\perp}{\sigma_j^\perp} = \frac{A'}{A''} \sqrt{\left(\frac{\frac{1}{\Delta t} \int_0^{\Delta t} (e^{-\lambda t} \cos(\omega t))^2 dt - }{\left(\frac{1}{\Delta t} \int_0^{\Delta t} e^{-\lambda t} \cos(\omega t) dt \right)^2} \right)} \quad (4.1)$$

where A' and A'' are the maximum amplitude during the main wave and the stable period, respectively, and Δt and T_1 are the duration of main waves and stable periods, respectively. Since σ_j^\perp are measured in stable periods, the result of the integration term in σ_{event}^\perp is irrelevant to the range of integration (T_1). In order to simplify the integration term in σ_j^\perp , we fix the time interval Δt (0.235) which is calculated by max speed 17m/s for the vehicle and average length 4m for the abnormality in our experiment. By this manipulation, Eq. 4.1 becomes a multiple of A'/A'' which is good for the abnormality index.

We compare the abnormality index of bumps measured by HTC desire and expansion joints measured by HTC desire and Sony Xperia S with fixed Δt and unfixed Δt and the results are shown in Figure 4.14, Figure 4.15 and 4.16, respectively.

We also split σ^\perp by speeds into 5 groups and calculate the average abnormality indexes for bumps and expansion joints as shown in Figure 4.17, and the Table 4.4 shows the standard deviation of the abnormality indexes for bumps and expansion joints with respect to the previous method and this method. The result shows that this way is better than the previous one. So, we modify our detection algorithm for a fixed $\Delta t = 0.235$ in the calculation of σ_{event}^\perp .

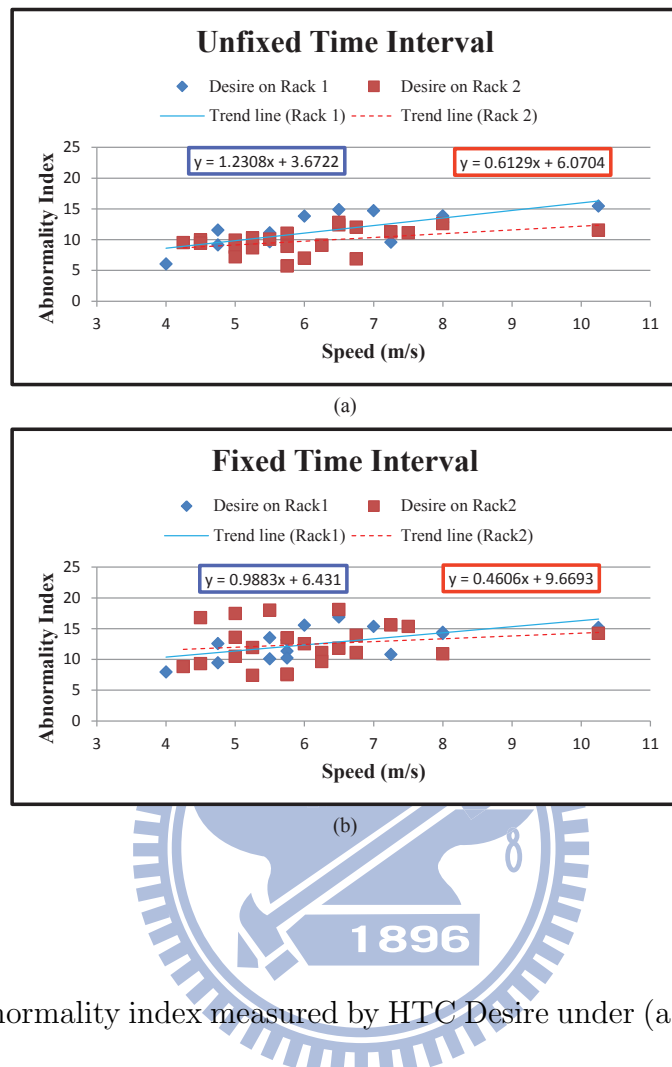


Figure 4.14: The abnormality index measured by HTC Desire under (a) unfixed time interval Δt and (b) fixed time interval Δt .

Table 4.4: The standard deviations of the abnormality indexes for bumps and expansion joints under unfixed and fixed time interval.

Standard Deviation	Unfixed	Fixed
Bump	1.43719132	1.43555212
Expansion Joint	1.0305563	0.8345104

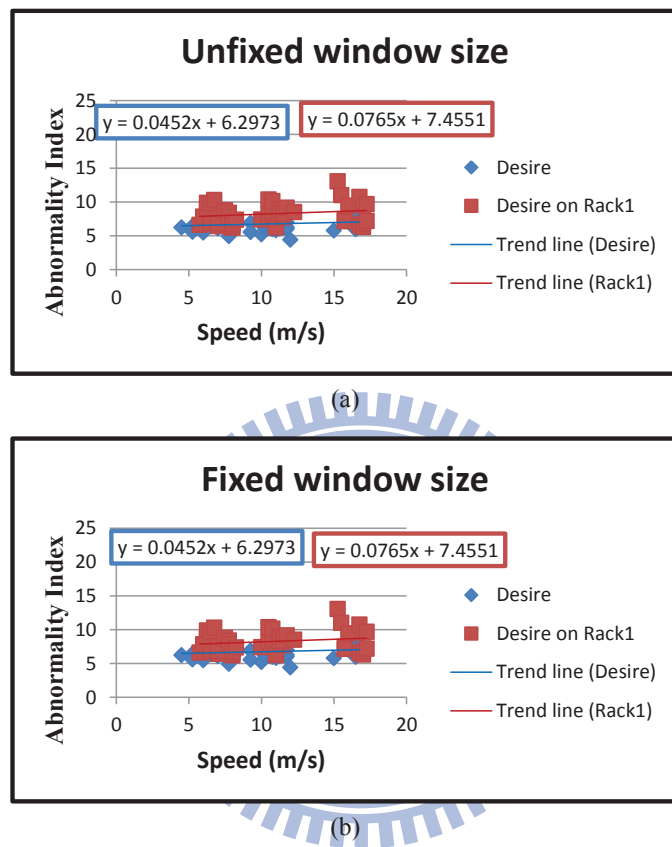


Figure 4.15: The abnormality index for expansion joints measured by HTC Desire under (a) unfixed time interval Δt and (b) fixed time interval Δt .

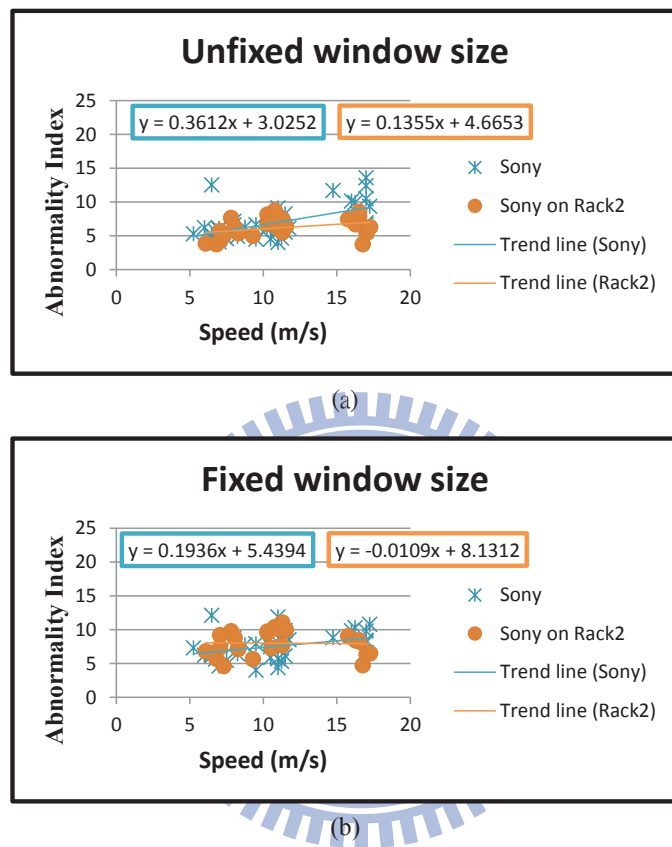
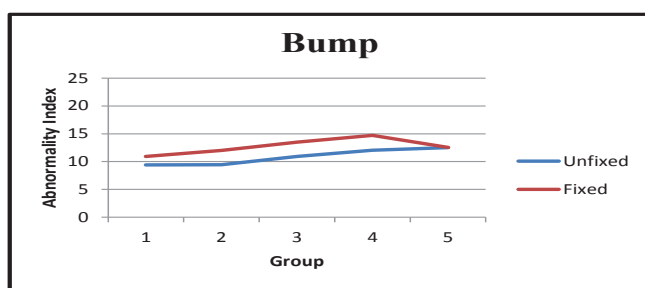
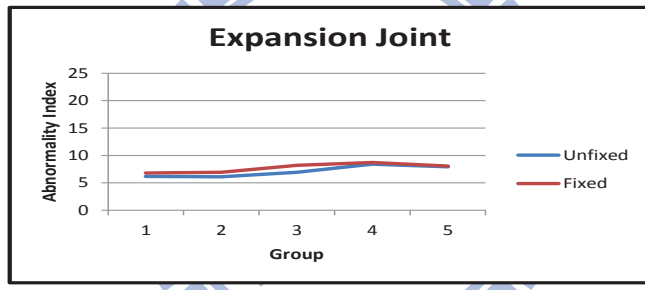


Figure 4.16: The abnormality index for expansion joints measured by Sony Xperia S under (a) unfixed time interval Δt and (b) fixed time interval Δt .



(a)

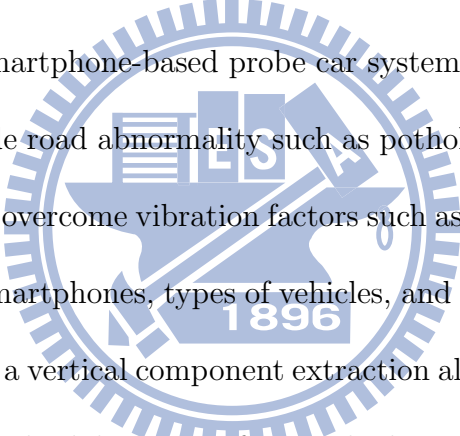


(b)

Figure 4.17: The average abnormality index for (a) bumps and (b) expansion joints.

Chapter 5

Conclusions

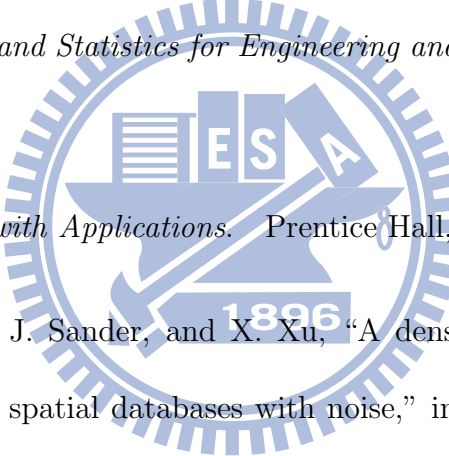


In this thesis, we propose a smartphone-based probe car system that utilizes mobile sensing to pervasively detect and grade road abnormality such as potholes, speed bumps, expansion joints manhole covers, etc. To overcome vibration factors such as orientation of smartphones, phone racks, sensor chips of smartphones, types of vehicles, and driving speed, several mechanisms are proposed including a vertical component extraction algorithm and an abnormality detection algorithm by the standard deviation of vertical vibration. The result indicates that our algorithm can eliminate these factors and grade the road abnormality.

Bibliography

- [1] *The Flatness of Roads Project Report (in Chinese)*. Taipei Government, April 2010, vol. 10, no. 7.
- [2] K. D. Zoysa, C. Keppitiyagama, G. P. Seneviratne, and W. W. A. T. Shihan, “A public transport system based sensor network for road surface condition monitoring,” in *ACM SIGCOMM workshop on Networked systems for developing regions (NSDR '07)*, 27 August 2007, pp. 9:1–9:6.
- [3] J. Eriksson, L. Girod, B. Hull, R. Newron, S. Madden, and H. Balakrishnan, “The pothole patrol: Using a mobile sensor network for road surface monitoring,” in *the 6th international conference on Mobile systems, applications and services (MobiSys 08)*, 17-20 June 2008, pp. 29–39.
- [4] P. Mohan, V. N. Padmanabhan, and R. Ramjee, “Nericell: Rich monitoring of road and traffic conditions using mobile smartphones,” in *the 6th international conference on Embedded network sensor systems (Sensys 08)*, 5-7 November 2008, pp. 357–358.

- [5] A. Mednis, G. Strazdins, R. Zviedris, G. Kanonirs, and L. Selavo, “Real time pothole detection using android smartphones with accelerometers,” in *2011 International Conference on Distributed Computing in Sensor Systems and Workshops (DCOSS)*, 27-29 June 2011, pp. 1 –6.
- [6] E. D. Kaplan and C. J. Hegarty, *Understanding GPS Principles and Applications*. Artech House, November 2006.
- [7] R. Bajaj, S. Ranaweera, and D. Agrawal, “GPS: location-tracking technology,” *Computer*, vol. 35, no. 4, pp. 92 –94, April 2002.
- [8] A. El-Rabbany, *Introduction to GPS: The Global Positioning System*. Artech House, August 2006.
- [9] “Crossbow Technology Inc. MPR-MIB users manual,” Website, 2006, <http://www.xbow.com>.
- [10] “HP iPAQ hw6965 Mobile Messenger Specifications,” Website, <http://h10010.www1.hp.com/wwpc/au/en/ho/WF06a/1090709-1113753-1113753-1113753-1117925-12573438.html>.
- [11] “SparkFun Wireless Accelerometer/Tilt Controller version 2.5,” Website, <http://www.sparkfun.com/commerce/productinfo.php?products.id=254>.

- [12] Y.-C. Tai, C.-W. Chan, and J. Y.-J. Hsu, “Automatic road anomaly detection using smart mobile device,” in *the 2010 Conference on Technologies and Applications of Artificial Intelligence (TAAI 2010)*, 18-20 November 2010.
- [13] “HTC,” Website, <http://www.htc.com/tw/>.
- [14] A. H. Nayfeh and D. T. Mook, *Nonlinear Oscillations*. Wiley-VCH, March 1995.
- [15] C. W. de Silva, *Vibration Damping, Control, and Design*. CRC Press, April 2007.
- [16] H. J. Pain, *The Physics of Vibrations and Waves*. Wiley, May 2005.
- [17] J. L. Devore, *Probability and Statistics for Engineering and the Sciences*. Duxbury Pr, December 1999.
- 
- [18] S. Leon, *Linear Algebra with Applications*. Prentice Hall, September 2009.
- [19] M. Ester, H.-P. Kriegel, J. Sander, and X. Xu, “A density-based algorithm for discovering clusters in large spatial databases with noise,” in *Published in Proceedings of 2nd International Conference on Knowledge Discovery and Data Mining (KDD-96)*, 2-4 August 1996.
- [20] A. Hinneburg and D. A. Keim, “An efficient approach to clustering in large multimedia databases with noise,” in *Proceedings of the 4th International Conference on Knowledge Discovery and Data Mining, AAAI Press*, 27-31 August 1998.